Draft version January 9, 2012
Preprint typeset using LaTeX style emulateapj v. 5/2/11

arXiv:1201.0939v2 [astro-ph.CO] 6 Jan 2012

QSO ABSORPTION SYSTEMS DETECTED IN NE VIII: EVIDENCE FOR HIGH-METALLICITY, MULTIPHASE GAS FAR FROM GALAXIES [1]

J.D. Meiring[2], T. M. Tripp[2], J. K. Werk[3], J.C. Howk [4], E.B. Jenkins[5], J. X. Prochaska[3], N. Lehner[6], K. R. Sembach[6]

Draft version January 9, 2012

ABSTRACT

Using high signal-to-noise spectra (S/N 30) taken with the Cosmic Origins Spectrograph (COS) of the z_{em}=0.9754 quasar PG1148+549, we report on the physical conditions of Ne VIII + OVI absorption line systems at z_{abs}=0.6838, 0.7015, 0.7248. At these redshifts, absorption lines from multiple ionization stages of oxygen (O II, O III, O IV, O VI) are available to constrain the ionization and physical conditions of the gas. A single-phase model with only photoionization or collisional ionization fails to reproduce the observed column density ratios. Even with extreme modifications to the ionizing background, single-phase photoionzation models fail to produce enough Ne VIII. We thus conclude that the O VI and Ne VIII are produced via collisional ionization. The metallicities of these systems are determined to be [O/H]> -0.5, higher than the typically assumed value for O VI absorbers of [O/H]~ -1.0. Densities of n$_H \sim 10^{-4}$ cm^{-3} are determined for the photoionized phase, indicating that these systems reside in regions of overdensity $\Delta \sim 80$. The collisionally ionized component of the gas traced by O VI and Ne VIII bears temperatures of T$\sim 10^{5.7}$ K. We determine the redshift density of Ne VIII absorbers d$\mathcal{N}$/d$z \sim 7^{+7}_{-3}$, similar to the redshift density of O VI absorbers of comparable equivalent width to these systems. Based on the redshift density and galaxy luminosity function at z$\sim$0.7, we estimate the cross section radius of the O VI + Ne VIII absorbers to be ∼70-150 kpc. We find a star forming ∼L* galaxy at the redshift of the z_{abs}=0.7248 system, at an impact parameter of 217 kpc.

Subject headings: Intergalactic Medium

1. INTRODUCTION

The cosmic baryon fraction has now been well constrained by both big bang nucleosynthesis coupled with deuterium measurements (O'Meara et al. 2006) as well as observations of the cosmic microwave background (Spergel et al. 2007) to be $f_b = 0.17 \pm 0.01$. At odds with the cosmological value, the baryon fractions in nearby galaxies as measured by their stellar and gas components compared to the dark matter mass are known to be well below the cosmic value (McGaugh et al. 2010). One explanation for these "missing" baryons is that low density gas residing in the halos of galaxies and groups is heated during infall into the potential well of the structure. This shock heating is a universal prediction of hydrodynamical simulations of structure formation (Davé et al. 2001; Cen & Fang 2006; Tepper-Garcìa et al. 2011). Alternatively, it is possible that the baryons never cool and fall into the dark matter halos as galaxies evolve (Maller & Bullock 2004; Anderson & Bregman 2010). In either case, the observations indicate that the majority of the baryons in the Universe are not located in the disks of galaxies. The most sensitive method to search for such low density plasmas currently is via the ultraviolet (UV) absorption lines imprinted on the spectrum of a background quasar (QSO).

Simulations and analytical models of galaxy formation and evolution require massive outflows to account for the observed properties of galaxies such as the stellar and ISM metallicities, as well as the total stellar masses. Similarly, the "closed box" model of galactic chemical evolution dramatically fails to reproduce the distribution of stellar metallicities in the Milky Way and nearby galaxies (Worthey et al. 1996; Schmidt 1963). Feedback processes from current or recent star formation, either through radiatively driven or supernova driven galactic scale winds are thought to play crucial roles in the evolution of a galaxy. Such outflows are commonly seen in nearby star forming galaxies (Heckman et al. 1995; Martin et al. 2002; Veilleux et al. 2005), and are thought to be responsible for injecting energy and mass into the circumgalactic medium (CGM) and beyond into the IGM.

The O VI λλ 1031.9, 1037.6 lines arising from O^{5+}, which has a peak ionization at ∼300,000 K in collisional ionization (Gnat & Sternberg 2007), have been used to trace hot gas in a range of environments from the local ISM to the IGM (Bowen et. al. 2008). Recent observations indicate that the extended halos of star forming galaxies are ubiquitously filled with oxygen and nearly all have detectable O VI absorption in the halos out to ∼150 kpc. This circumgalactic material appears to contain a substantial amount of mass, comparable to the

---

[1] Based on observations made with the NASA/ESA Hubble Space Telescope, obtained at the Space Telescope Science Institute, which is operated by the Association of Universities for Research in Astronomy, Inc., under NASA contract NAS 5-26555. These observations are associated with program GO11598.

[2] Department of Astronomy, University of Massachusetts, Amherst, MA 01003, USA
[3] University of California Observatories-Lick Observatory, UC Santa Cruz, CA 95064, USA
[4] Department of Physics, University of Notre Dame, 225 Nieuwland Science Hall, Notre Dame, IN 46556, USA
[5] Princeton University Observatory, Peyton Hall, Ivy Lane, Princeton, NJ 08544, USA
[6] Space Telescope Science Institute, 3700 San Martin Drive, Baltimore, MD 21218, USA

Table 1
Cosmic Origins Spectrograph Observations of PG1148+549

COS Grating	λ_{cen} (Å)	Observation Date	Exposure Time (seconds)	MAST ID[a]
G130M	1309	2009 Dec. 30	3192	LB1O22Q3Q
G130M	1309	2009 Dec. 30	3192	LB1O22RAQ
G130M	1309	2009 Dec. 30	2527	LB1O22PMQ
G130M	1327	2009 Dec. 26	2527	LB1O23EBQ
G130M	1327	2009 Dec. 30	3192	LB1O22RHQ
G130M	1327	2009 Dec. 30	3192	LB1O22RRQ
G160M	1600	2009 Dec. 26	3192	LB1O23EOQ
G160M	1600	2009 Dec. 26	3192	LB1O23EFQ
G160M	1600	2009 Dec. 26	3192	LB1O23EVQ
G160M	1623	2009 Dec. 25	2482	LB1O24ACQ
G160M	1623	2009 Dec. 25	3192	LB1O24AFQ
G160M	1623	2009 Dec. 26	3192	LB1O23F2Q

[a] Exposure identification code in the Multimission Archive at Space Telescope (see http://archive.stsci.edu/index.html).

mass of the ISM in the galaxy itself (Tumlinson et al. 2011b; Tripp et al. 2011; Prochaska et al. 2011).

Hydrodynamical simulations of galaxy evolution show that O VI absorbers typically reside in metal enriched regions with overdensities $\Delta = \rho/\langle\rho\rangle$ of 1−100 (Cen & Fang 2006; Davé et al. 2001; Tepper-Garcìa et al. 2011; Oppenheimer & Davé 2009; Oppenheimer et al. 2011; Smith et al. 2011). Simulations by Tepper-Garcìa et al. (2011) indicate that O VI does appear to trace primarily shock heated gas, with the distribution of temperatures peaked at $\sim 10^{5.3}$ K. However, ∼30 percent of the O VI systems in that simulation are at lower temperatures, and primarily ionized by the local UV background. Other simulations indicate that the O VI and even Ne VIII absorbers arise primarily in photoionized gas (Oppenheimer & Davé 2009; Oppenheimer et al. 2011). Interestingly, ∼ 30% of the observed O VI absorbers have characteristics of cool, photoionzed gas (Tripp et al. 2008).

Despite recent advances in the UV spectroscopy of the low-z IGM, several questions are still unanswered due in part to the lack of diagnostic lines at low redshift. The baryonic content is still largely unknown, as well as the metallicity and ionization mechanisms of the gas comprising the IGM and CGM. Much of the work on low-z absorption lines has been accomplished with the *Space Telescope Imaging Spectrograph* (STIS) and *Far Ultraviolet Spectroscopic Explorer* (FUSE) spectrographs, which are sensitivity limited to the brightest QSOs and hence lowest redshifts. At these redshifts, few absorption lines are available and much of the determination of the physical conditions in the systems is forced to be based on H I and O VI alone, or based on column density ratios of different ions such as C III and Si III. As such, non-solar abundance ratios of the different elements can be mistaken for the effects of ionization.

In order to overcome some of these issues and to better constrain the physical conditions in the IGM and CGM, we have undertaken a blind survey of $z \sim 1$ QSOs with the COS spectrograph (Froning & Green 2009; Green et al. 2011). At moderate redshifts, we can access many of the numerous absorption lines in the FUV at $\lambda <$ 912 Å. Multiple transitions of other ionization states of oxygen are well as many other ions are available at 600−1000 Å in the rest frame (Verner et al. 1994). At $z \sim 0.5$, these transitions enter the bandpass of the Cosmic Origins Spectrograph (COS) onboard the *Hubble Space Telescope* (HST).

Aside from O VI, other ions of highly ionized species exist with absorption lines in the FUV. The Ne VIII $\lambda\lambda$ 770,780 doublet enters the COS bandpass at $z \sim 0.45$. The ionization potential of Ne^{+6} is 207 eV; as such Ne VIII is expected to be a more reliable tracer of collisionally ionized gas. Several absorption systems bearing Ne VIII have been discovered, indicating highly ionized and multiphase gas with temperatures of T=10^{5-6} K. (Savage et al. 2005; Narayanan et al. 2009, 2011; Tripp et al. 2011).

The excellent sensitivity of COS in the UV gives the opportunity to study the IGM and CGM in much more detail than has ever been achievable in the past. In this work we study in detail absorption systems at $z \sim 0.7$ where we have access to a number of ionization states of oxygen (O I to O VI) and the Ne VIII $\lambda\lambda$ 770, 780 doublet towards PG1148+549. The organization of the paper is as follows: In § 2, we discuss the COS observations and data handling, details of the analysis of each absorption system are given in § 3, § 4 describes the ionization modeling, results are given in § 5, a discussion of the galaxies in the field are given in § 6, and § 7 gives a summary and discussion.

2. OBSERVATIONS

The observations presented here were taken as part of program GO11741 (PI Tripp), a blind survey of $z \sim 1$ UV-bright quasars in search of highly ionized species such as O VI, Ne VIII, and Mg X as well as the multiphase halos of galaxies. Targets for this sample have been selected only based on their redshift ($z \gtrsim 1$) and flux in the far ultraviolet (FUV). PG1148+549 was previously observed with the *Faint Object Spectrograph* (FOS, $R \sim 1300$) in programs 4952 and 6210, although the resolution and S/N are far too low for the purposes of the analysis in this work. These COS spectra were acquired on 25-30 December 2009 and cover a wavelength range of 1150-1800 Å. Details of the COS observations are given in Table 1.

These data were processed in the same manner as described in Meiring et al. (2011). Multiple focal-plane positions were used to reduce the effects of fixed-pattern noise when the various exposures were combined. In addition, flatfielding was applied. The reduced and coadded spectra have been binned by 3 pixels, as the raw COS data are oversampled with a ∼ 6 pixel wide resolution element. All subsequent measurements and analysis were performed on the binned spectra. The binned spectra have a resolution of ∼15 km s^{-1} per resolution element and have been normalized using a cubic spline function to fit the continuum. The S/N of these COS spectra range from $20 - 40$ per resolution element.

3. NOTES ON INDIVIDUAL SYSTEMS

A number of absorption line systems are observed in the spectrum of PG1148+549. Here, we focus on three systems at $z = 0.6883, 0.7015, 0.7248$ with Ne VIII detections as this redshift allows for the multiple ionization stages of oxygen as well as the Ne VIII

$\lambda\lambda$ 770,780 doublet to be observable. Other absorption systems with multiple lines have been identified at z_{abs}=0.2552,0.5778,0.5910.

We have used profile fitting to determine column densities in the absorption lines detected in the PG1148+549 spectrum. The synthetic Voigt profiles were convolved with the COS line spread functions (LSF)[7] as determined by the COS science team at the nearest tabulated wavelength (Ghavamian et al. 2009). Whenever possible, multiple transitions were fit simultaneously (e.g. Lyman β, Lyman γ, Lyman δ) to determine the best fitting column densities. Upper limits on column densities for non-detected species were determined in the manner described in Meiring et al. (2011). In short, synthetic Voigt profiles are created and the column density is increased until a 3σ limit is indicated given the S/N of the data.

The COS wavelength solution is now known to have inaccuracies on one to two pixel levels (i.e. up to $\sim$ 30 km s^{-1}), especially at the wavelength extremes of the instrument (Savage et al. 2011). Shifts in velocity of this order have been applied to the absorption lines when necessary. The solar system abundances used throughout this paper have been adopted from Lodders (2003).

3.1. *The z_{abs}=0.6838 system:*

Velocity plots for the lines are shown in Figure 1, with the best fit profiles overlayed in red. We have used two components to fit the absorption lines in this system. The Lyman α λ 1215 line falls outside of the COS bandpass, however we detect transitions from Lyman β λ 1025 to Lyman ϵ λ 937. Further transitions in the Lyman series are too weak to detect.

Multiple metal lines are also detected. Lines of O IV λ 787, O VI $\lambda\lambda$ 1031, 1037, N IV λ 765, and C III λ 977 are all detected at high significance. The O III λ 832 line is blended with the Milky Way Si IV λ 1402 line. By fitting the corresponding Si IV λ 1393 line, we have removed this contamination from the O III λ 832 profile. A strong Lyman α line at z_{abs}=0.1529 is also observed at -175 km s^{-1}. This was also included in the fit to the O III line as some optical depth may be contaminating the profile due to the extended wings of the COS LSF. The fit to the O III λ 832 line in Figure 1 shows the contribution from Milky Way Si IV λ 1402 with the thick orange line.

Comparisons of the apparent column density $N_a(v)$ profiles using the apparent optical depth method of Savage & Sembach (1991) are shown in Figures 2 and 3. The O IV and O VI profiles show excellent agreement in the component structure as can be seen in Figure 2. The apparent optical depth of the O IV λ 787 line has been scaled by a factor of 0.75 for the sake of comparison. Column densities via the apparent column density method and equivalent widths are given in Table 3, while the adopted column densities determined via profile fitting are given in Table 2.

The Ne VIII λ 780 line is blended with a C III λ 977 line at z_{abs}=0.5778. As this is the only C III line available, it is impossible to remove the contamination from the Ne VIII λ 780 line. The Ne VIII λ 770 line is not blended with any other features, and we determine a column density of log N(Ne VIII)=14.14±0.04 via profile fitting. The Ne VIII λ 770 line is well aligned with the O VI λ 1031 line, as can be seen in Figure 3, increasing our confidence in the veracity of the Ne VIII detection. This gives the ratio of N(Ne VIII)/N(O VI)$\sim$0.42.

3.2. *The z_{abs}=0.7015 system:*

No Lyman series absorption lines are detected in this system. We place an upper limit on N(H I) based on the non-detection of the Lyman β λ 1025 line of log N(H I)<13.8. Velocity plots of the absorption lines from this system are shown in Figure 4, with the best fit profiles overlayed in red.

Multiple metal lines are detected in this system. Lines of O III λ 832, O IV λ 787, O VI $\lambda\lambda$ 1031,1037, C III λ 977, and Ne VIII $\lambda\lambda$ 770,780 are all detected. The Ne VIII $\lambda\lambda$ 770,780 lines have a doublet ratio of 2:1, assuming the lines are weak and lie on the linear portion of the curve of growth the equivalent widths of the lines should have the same ratio. We find $W_0(770)$=28±5 mÅ and $W_0(780)$=18±6 mÅ including errors from continuum placement and photon noise. The observed ratio of 1.6:1 is close to the expected value, and there appears to be some contamination in the λ 780 line in the red side of the profile which could account for the increased optical depth. The profiles do match well in terms of alignment in velocity space, as can be seen in Figure 7.

Two components were used to fit the profiles at $v = +3$ and $v = +63$ km s^{-1} relative to the systemic redshift of the system. The strongest component in each line is centered at $v = +3$ km s^{-1}. Apparent optical depth profiles of the O IV, O VI, and Ne VIII lines are shown in Figures 6 and 7. The O IV profile has been scaled by a factor of 1.5 for comparison to the O VI lines in Figure 6.

N III is not detected in this system, the N III λ 989 line is blended with a Lyman α line at z_{abs}=0.3862, and the N III 685 line, which is nearly two times stronger, is not observed as well. The N IV λ 765 line, the only N IV line available at these redshifts, is unfortunately blended with the strong Galactic absorption line of O I λ 1302.

With a simultaneous fit of the O VI $\lambda\lambda$ 1031,1037 lines using two components in each line, we determine log N(O VI)=14.37±0.05 combined in the two components. The Ne VIII $\lambda\lambda$ 770,780 lines were also fit simultaneously giving log N(Ne VIII)=13.86±0.05. This gives a ratio of N(Ne VIII)/N(O VI)$\sim$0.30. Column densities via the apparent column density method and equivalent widths are given in Table 5, while the adopted column densities determined via profile fitting are given in Table 4.

3.3. *The z_{abs}=0.7248 system:*

No Lyman series absorption lines are detected in this system. We place an upper limit on N(H I) based on the non-detection of the Lyman β λ 1025 line of log N(H I)<13.7. Figure 5 shows multiple lines of interest in the system.

The O IV λ 787 and O VI $\lambda\lambda$ 1031, 1037 lines are detected in this system at high significance. A single component centered at $v = -4$ km s^{-1} relative to the systemic redshift of z_{abs}=0.7248 was used to fit the profiles. The adopted column densities determined via profile fitting are given in Table 6.

---

[7] Tabulated LSFs for COS are available at `http://www.stsci.edu/hst/cos/performance/spectral_resolution/`

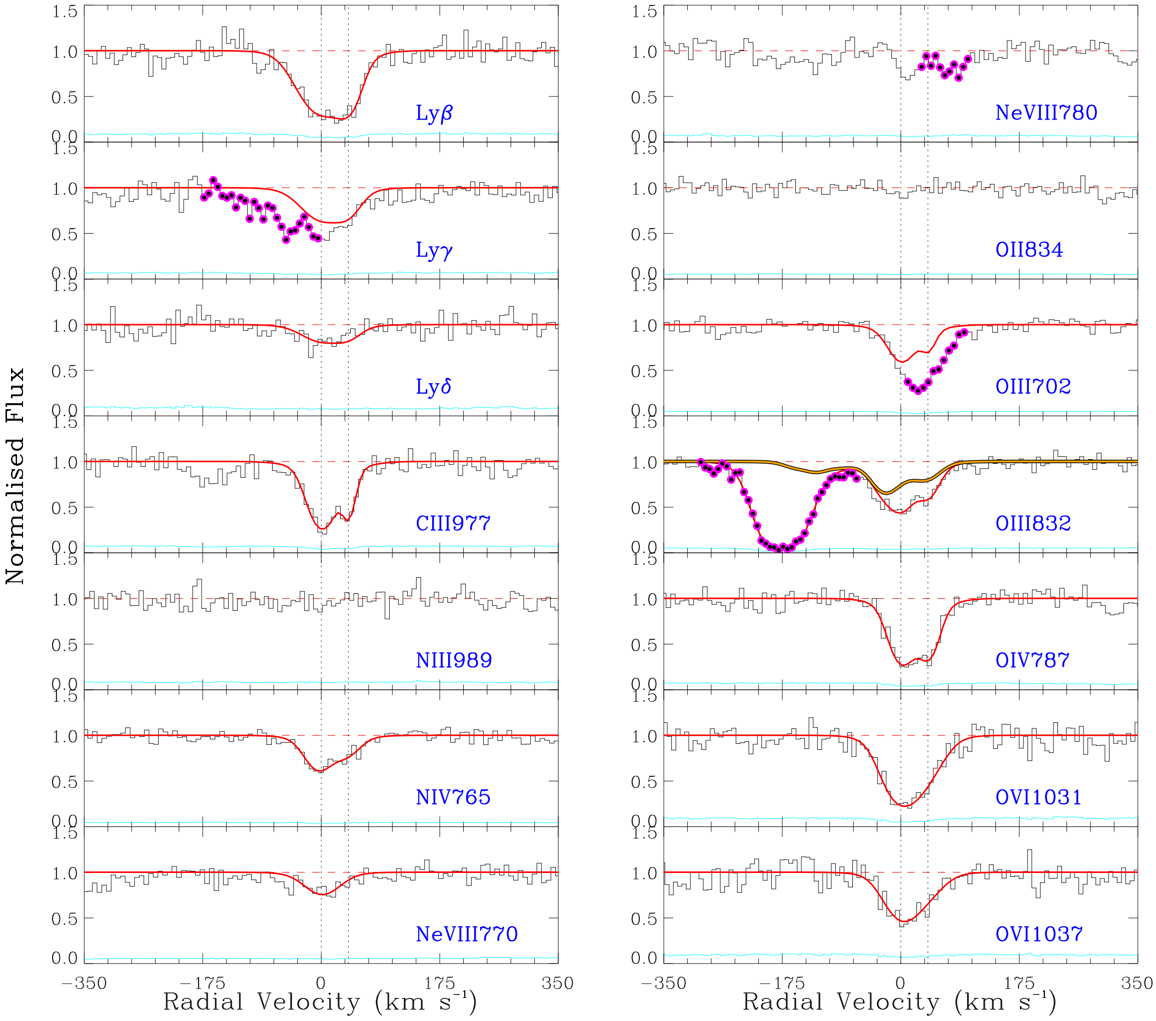

Figure 1. Velocity plots of the absorption lines in the z_{abs}=0.6838 system in PG1148+549. Vertical dotted lines mark the positions of the components. The solid red line represents the best fit models determined from profile fitting. The O III λ 832 line is partially blended with the Si IV λ 1402 line from the Milky Way. The contribution from Si IV λ 1402 is shown with the solid orange line. Magenta point denote regions where the lines are blended with unaffiliated features from other systems. The cyan line at the bottom of each panel denotes the 1σ error of the normalized flux.

Two features are located at the expected positions of the Ne VIII $\lambda\lambda$ 770,780 lines with S/N∼30 per resolution element in the region giving EW(770)=26±8 mÅ and EW(780)=19±5 mÅ Profile fitting of the lines gives log N(Ne VIII)=13.81±0.07, and a ratio of N(Ne VIII)/N(O VI)=0.89 indicating a high temperature if the gas is in collisional ionization equilibrium.

The N IV λ 787 and C III λ 977 lines are heavily blended with features from other systems, and could not be fit. Apparent column density profile plots of the O IV, O VI and Ne VIII profiles are shown in Figures 8 and 9. Column densities via the apparent column density method and equivalent widths are given in Table 7.

4. IONIZATION MODELING

4.1. *Photoionization*

A large suite of ions is necessary to constrain photo or collisional ionization models. As most of the O VI absorbers observed to date are at lower redshift, the number of species available is limited to H I, O VI, Si III, C III and/or C IV in most cases. In a limited number of cases, a wider array of ions has been presented (e.g. Chen & Prochaska (2000); Sembach et al. (2004); Lehner et al. (2009)).

The carbon to oxygen ratio is known to vary as a function of metallicity, with carbon being sub-solar at the ∼0.5 dex level for [O/H]< −0.5 (Akerman et al. 2004; Pettini et al. 2008). The N V $\lambda\lambda$ 1238,1242 lines are also sometimes seen in the IGM, and have also been used to constrain ionization models. The [N/O] ratio is also well known to be metallicity dependent in H II regions in the Milky Way and nearby galaxies (Van Zee et al. 1998; Van Zee & Haynes 2006). As such, the observed ratios of carbon to oxygen and nitrogen to oxygen in ionized

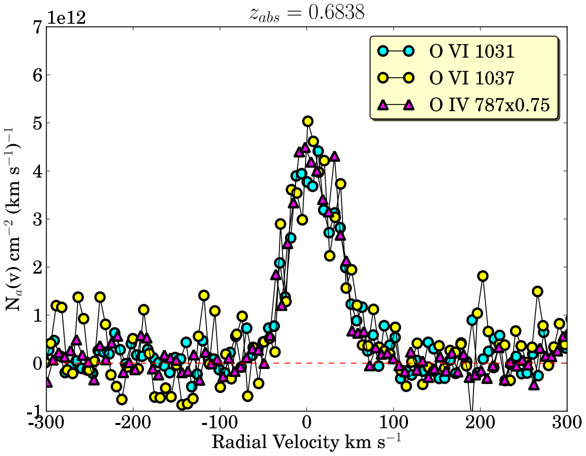

Figure 2. Apparent column density profiles of the O IV and O VI lines from the z_{abs}=0.6838 system. The O IV λ 787 line has been scaled by a factor of 0.75 for illustration.

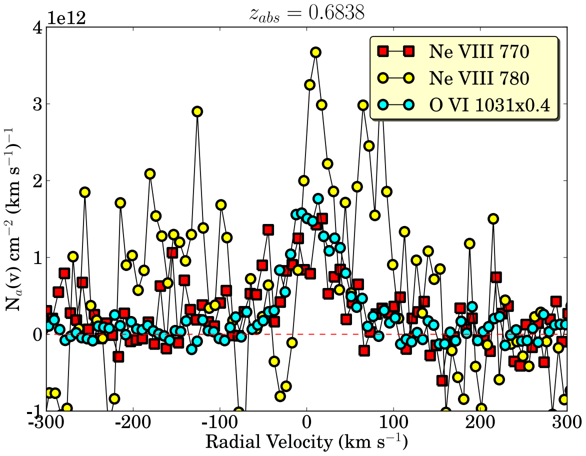

Figure 3. Apparent column density profiles of the O VI and Ne VIII lines from the z_{abs}=0.6838 system. The O VI λ 1031 line has been scaled by a factor of 0.4 for illustration.

Table 2
Adopted column densities from profile fits to the COS data for the z_{abs}=0.6838 system.

Ion	v_{rad} km s^{-1}	log N cm^{-2}	b km s^{-1}
H I	+2	14.65 ±0.02	39.9±2.4
	+42	14.24±0.05	20.0±3.2
C III	+2	13.57±0.02	22.5±1.7
	+42	13.16 ±0.07	8.5±2.2
N III		< 13.5	
O II		< 13.3	
O III	+2	14.02±0.03	20.5[a]
	+42	13.64±0.06	16.2[a]
O IV	+2	14.49±0.03	20.5±1.8
	+42	14.28±0.04	16.2±2.0
O VI	+2	14.41±0.02	31.5±1.9
	+42	13.88±0.06	31.0±5.0
N IV	+2	13.32±0.05	23.9±2.7
	+42	12.96±0.07	22.1±5.3
Ne VIII	+2	13.95±0.04	32.0±5.0
	+42	–	–

[a] Due to the blending in this line, the b values for the components were fixed to the values determined from the O IV λ 787 line.

Table 3
Equivalent widths and AOD column densities for transitions observed in the z_{abs}=0.6838 system.

Transition	W_0 mÅ	N_a (AOD) cm $^{-2}$
H I 1025	276±17	14.77±0.02
H I 972	246±18[a]	<15.12
H I 949	54±15	14.74±0.11
H I 937	37±9	14.82±0.09
C III 977	188±12	13.65±0.02
O III 832	148±7[a]	< 14.47
N IV 765	80±8	13.47±0.04
O IV 787	153±8	14.60±0.02
O VI 1031	234±19	14.47±0.03
O VI 1037	149±23	14.50±0.06
Ne VIII 770	51±12	13.98±0.09
Ne VIII 780	59±11[a]	< 14.39

[a] Blended

Table 4
Measured column densities from profile fits to the COS data for the z_{abs}=0.7015 system

Ion	v_{rad} km s^{-1}	log N cm^{-2}	b km s^{-1}
H I		< 13.8	
O II		< 13.2	
C III	+4	13.39±0.03	23.9±2.2
	+63	12.63±0.10	18.7±6.9
N III		< 13.2	
O III	+4	13.55±0.06	23.9±5.5
	+63	–	–
O IV	+4	14.17±0.02	23.7±1.9
	+63	13.33±0.15	42.7±21.0
O VI	+4	14.28±0.03	20.9±2.0
	+63	13.63±0.12	27.3±10.3
Ne VIII	+4	13.86±0.05	27.8±3.5
	+63	–	–

Table 5
Equivalent widths and AOD column densities for transitions observed in the z_{abs}=0.7015 system.

Transition	W_0 mÅ	N_a (AOD) cm $^{-2}$
H I 1025	<30	< 13.8
C III 977	126±16	13.41±0.05
O III 832	18±5	13.48±0.09
O IV 787	75±9	14.18±0.04
O VI 1031	168±19	14.29±0.04
O VI 1037	113±19	14.35±0.06
Ne VIII 770	28±5	13.75±0.07
Ne VIII 780	18±6	13.86±0.11

Table 6
Measured column densities from profile fits to the COS data for the z_{abs}=0.7248 system.

Ion	v_{rad} km s^{-1}	log N cm^{-2}	b km s^{-1}
H I		< 13.7	–
N III		< 13.3	–
O III		< 13.5	–
O IV	−4	13.75±0.04	16.1±2.9
O VI	−4	13.86±0.07	15.8±3.8
NeVIII	−4	13.81±0.06	41.4±7.5

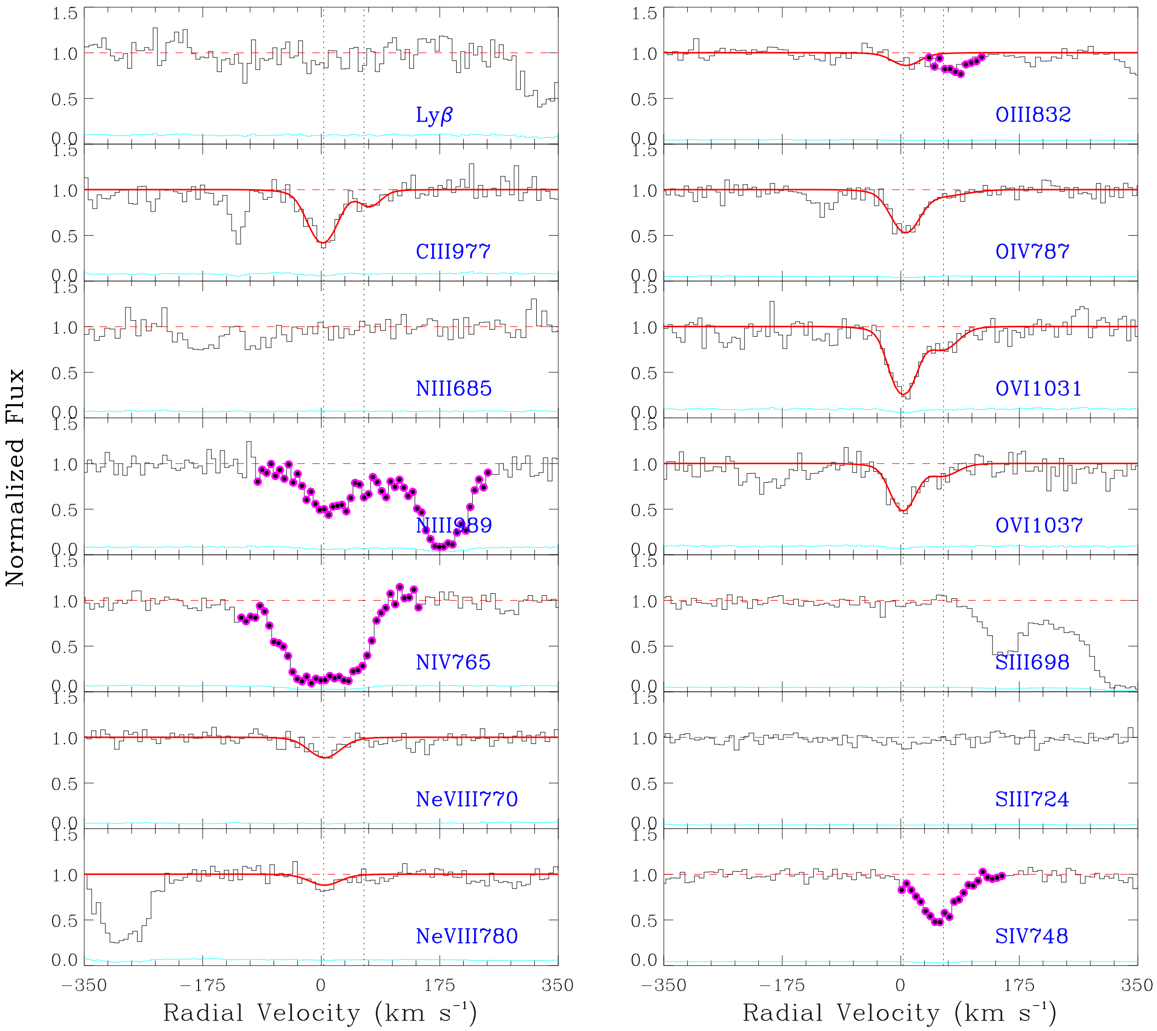

Figure 4. Same as Figure 1, but for the z_{abs}=0.7015 system.

Table 7
Equivalent widths and AOD column densities for transitions observed in the z_{abs}=0.7248 system.

Transition	W_0 mÅ	N_a (AOD) cm $^{-2}$
H I 1025	<30	< 13.7
O II 834	<15	< 13.5
O III 832	<16	< 13.5
O IV 787	27±5	13.70±0.06
O VI 1031	71±20	13.84±0.10
O VI 1037	37±12	13.87±0.15
Ne VIII 770	26±8	13.70±0.12
Ne VIII 780	19±5	13.87±0.10

plasmas are dependent on the metallicity as well as the temperature or ionizing flux, and make it rather difficult to tightly constrain parameters in the models.

The optimal solution is to have a number of adjacent ions from a single species, such as oxygen for which there are a number of lines from different ionization states in the FUV. Nitrogen and sulfur also have a number of resonance lines from multiple ionization states in the FUV, although the abundances of nitrogen and sulfur are lower than that of oxygen by a factor of ~ 7 and $\sim$32, respectively, making the detection of the lines more challenging.

To investigate the ionization mechanism in these systems we have created grids of photoionization models using CLOUDY version 10.00, last described in Ferland et al. (1998). We have used the Haardt & Madau extragalactic background spectrum (Haardt & Madau 1996), with the modifications and updates described in (Haardt & Madau 2001) at $z = 0.7$ including contributions from both AGN and galaxies to illuminate the plane-parallel clouds with ionizing radiation.

We have matched the observed O III to O IV ratio to the models in order to constrain the ionization parameter U, which is the ratio of the number density of ionizing photons to the particle density $U = n_\gamma/n_H$. The photon energy required to produce O^{3+} of 54.9 eV is just at the He^{+} ionization potential of 54.4 eV. The atmospheres of O and B type stars produce photons at these ener-

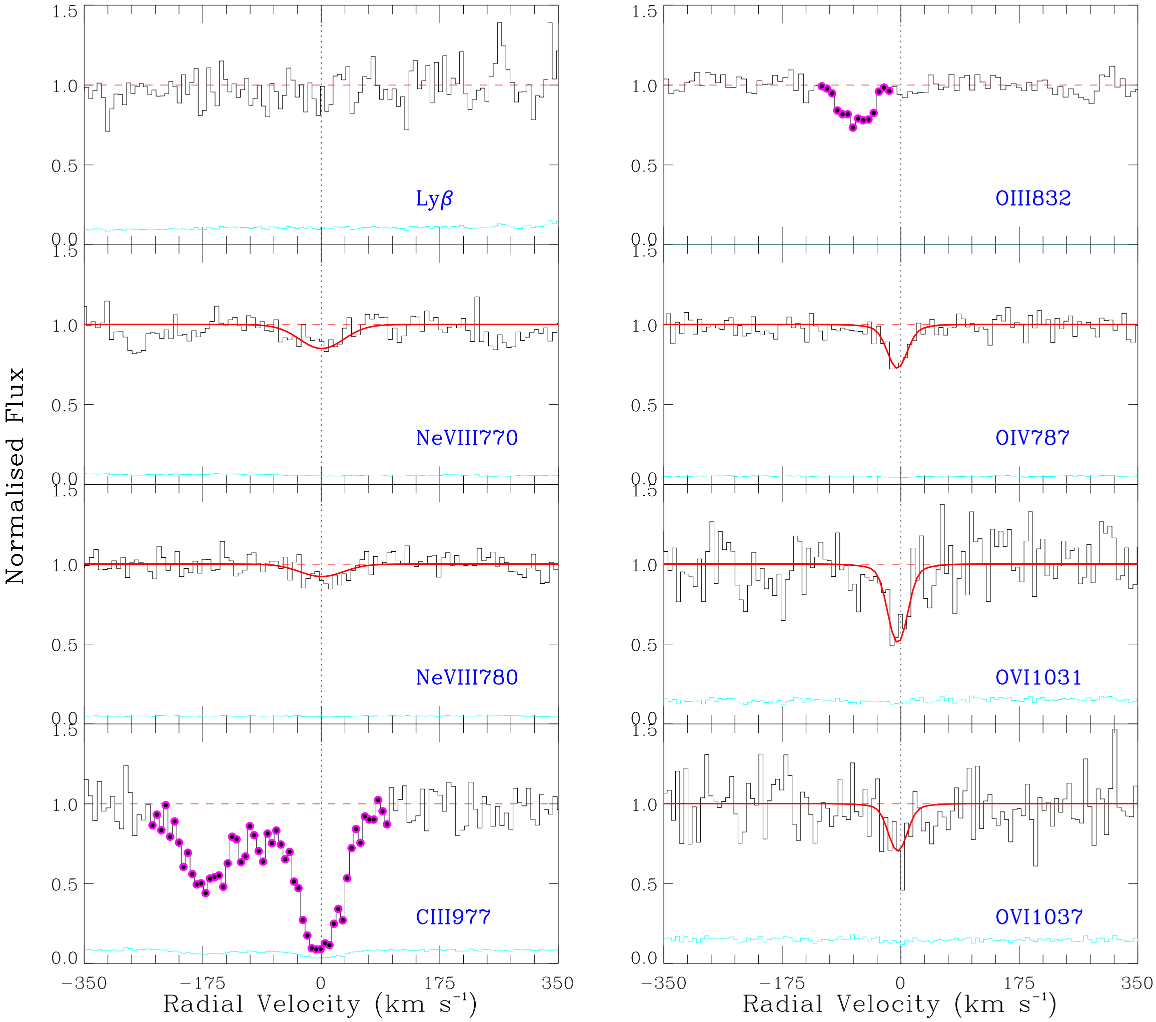

Figure 5. Same as Figure 1, but for the z_{abs}=0.7248 system.

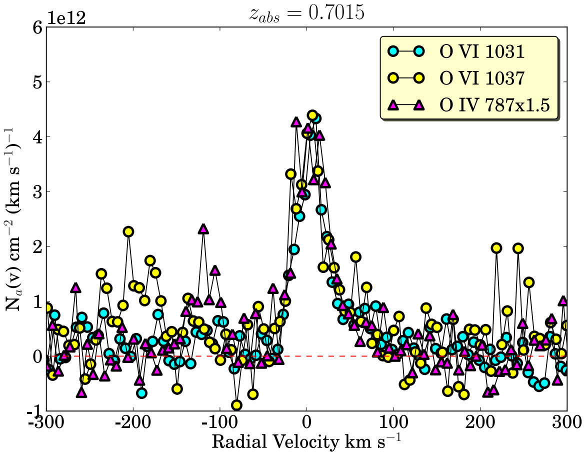

Figure 6. Apparent column density profiles of the O IV and O VI lines from the z_{abs}=0.7015 system. The O IV λ 787 line has been scaled by a factor of 1.5 for illustration.

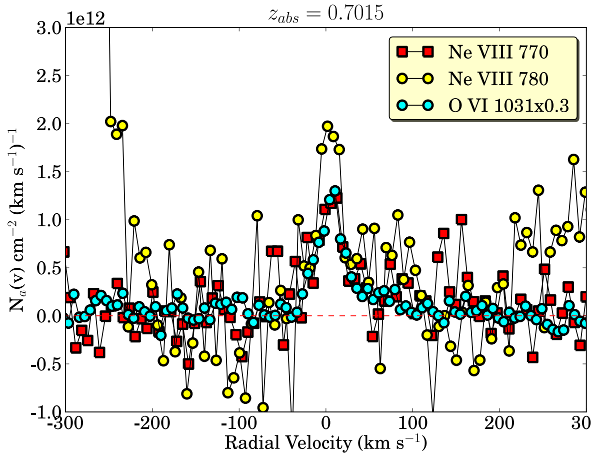

Figure 7. Apparent column density profiles of the O VI and Ne VIII lines from the z_{abs}=0.7015 system. The O VI λ 1031 line has been scaled by a factor of 0.3 for illustration.

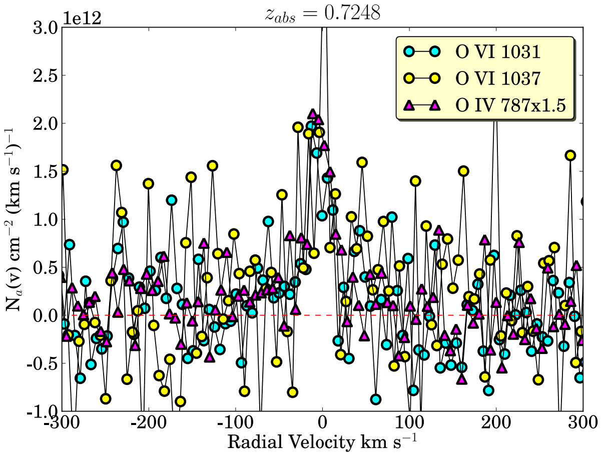

Figure 8. Apparent column density profiles of the O IV and O VI lines from the z_{abs}=0.7248 system. The O IV λ 787 line has been scaled by a factor of 1.5 for illustration.

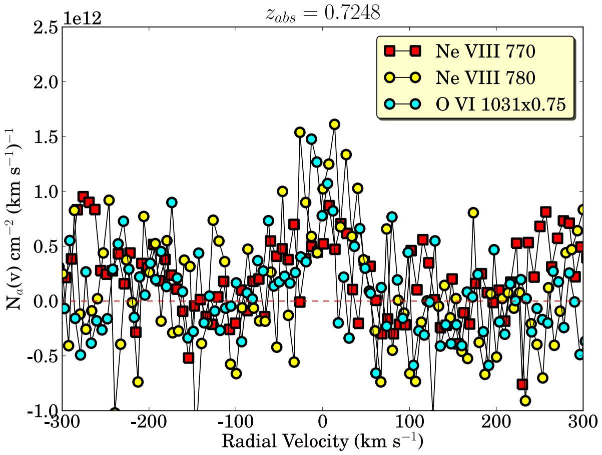

Figure 9. Apparent column density profiles of the O VI and Ne VIII lines from the z_{abs}=0.7248 system. The O VI λ 1031 line has been scaled by a factor of 0.75 for illustration.

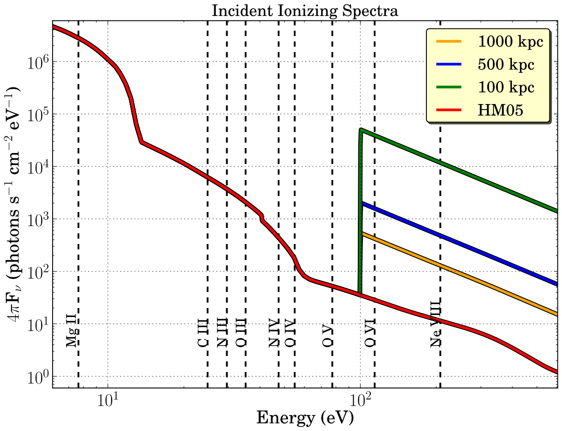

Figure 10. The extragalactic background spectra from Haardt & Madau (2001) in red, along with the modifications including an obscured AGN. Ionization potentials for several atoms included in the analysis of these absorbers are overplotted.

gies, wheres at higher energies the photon flux steeply declines due to absorption from He$^+$. Several lines of O II are covered in the data, although none are detected at adequate significance in any system and only weak upper limits can be placed on the columns density which do not constrain the models.

In Figure 11 we show the results of the CLOUDY photoionization models. For both the z_{abs}=0.6838 and z_{abs}=0.7015 systems the ionization parameter that best fits the O III and O IV column densities is log U=-1.5. The O VI and Ne VIII column densities are severely underestimated at the ionization parameter best fitting the O III to O IV ratio. There is no solution that fits the O III, O IV, and O VI column densities simultaneously. O III is underproduced in the models matching O IV and O VI, while O VI is underproduced when O III and O IV are matched.

As the O III λ 832 line was not detected in the z_{abs}=0.7248 system, we cannot place a unique value on the ionization parameter. We can however constrain the ionization parameter to a limited range. The observed ratio of O IV/O III>1.77 implies that log U> -1.75, while the observed ratio of O VI/O IV=1.29 bounds the ionization to be log U< -0.75. This allowed region is shaded in pink in the bottom row of Figure 11.

The close alignment between the low and high ions in these systems perhaps indicates a single-phase gas. As the Haardt & Madau (2001) background does not produce the column density ratios observed in these systems, is it possible to modify the ionizing background spectrum to produce the amount of high ions observed in these systems?

The UV background is particularly uncertain in the soft X-Ray regime (100-500 eV), where these photons are easily absorbed by Galactic gas. In order to investigate whether modifications to the Haardt & Madau ionizing background could reproduce the observed column density ratios, we have also created similar grids of models with various spectral energy distributions (SEDs) in order to investigate whether alterations to the ionizing spectrum can produce the observed column densities.

First, we have used the X-Ray emission from a solar metallicity 0.25 keV plasma, simulating the emission from the hot X-Ray emitting gas around nearby star forming galaxies which have been measured to have similar temperatures (Li et al. 2008). Such optically thin plasma does emit in the soft X-Rays, and is not included in the determination of the UV background of (Haardt & Madau 2001). This spectral energy distribution is dominated by emission lines, with some contribution from thermal continuum emission as well.

The typical luminosity of an X-Ray emitting halo is $\sim 10^{40}$ erg s^{-1} (Li et al. 2008). We model the clouds as plane parallel slabs outside of this X-Ray emitting halo. We find that O VI and Ne VIII are not produced at the ratios observed in these systems until the flux reaches $\sim 2.5 \times 10^{-3}$ erg s^{-1} cm^{-2}, implying a distance from the source of $\sim$ 0.2 kpc, assuming that the emission comes from a point source. In a real X-Ray emitting halo, the maximum flux is obviously lower as the emission arises in an extended volume. Nonetheless, such a small impact parameter is unphysical hence we rule this model out as a viable method to produce these high ions via photoionization.

We have also attempted to modify the Haardt & Madau (2001) background spectrum with the inclusion of an obscured AGN. With a total column density of $\sim 10^{19}$ cm^{-2}, the spectrum of an AGN will have a cutoff at ~ 0.1 keV due to the photoelectric absorption of the neutral gas. This is just below the ionization potential of O^{4+}, and the low energy cutoff is introduced here was chosen specifically to generate a boosted flux in this energy range. We have used a power law spectrum with the fiducial value of the spectral index $\alpha = 2.0$. Including such a source will allow for extra photon flux in soft X-Rays which are capable of creating O VI and Ne VIII while keeping the photon flux low at longer wavelengths.

Three models were created, with varying amounts of contribution to the soft X-Ray regime by increasing the intensity of the obscured AGN relative to the Haardt & Madau (2001) background. At a distance of 100, 500, and 1000 kpc from an AGN with a typical luminosity of 10^{45} erg s^{-1}, the AGN continuum will dominate the Haardt & Madau (2001) background by a factor of $\sim$1000, 40, and 10 respectively. These incident spectra are shown in Figure 10.

Again, even with the increased flux at the ionization potentials for the high ions, the column density ratios predicted in the photoionization simulations do not match the observed values. As such, we are forced to assume that the gas has multiple phases.

Could the high ions exist in a low density photoionized state? Such two phase photoionization models could potentially create a solution without a need for introducing a hot phase that is collisionally ionized. Problems arise however when investigating the sizes of the clouds in this scenario. The observed ratio of N(Ne VIII)/N(O VI) is reached when log $U \sim -0.25$ for these systems, which in turn implies densities of $\sim 1 \times 10^{-5}$ and sizes of > 1 Mpc. Such large structures would be affected by Hubble broadening of $\gtrsim 100$ km s^{-1}, which is not supported by the best fitting Doppler parameters. Similar arguments have also been made for other systems with Ne VIII detections, where the implied cloud sizes in the case of photoionization production of Ne VIII lead to unrealistically large cloudy sizes (Narayanan et al. 2011).

As single-phase, and even two phase photoionization models fail to account for both the low and high ions simultaneously, we are forced to conclude that the lower ions (O III, C III, O IV, etc.) reside in a photoionized core, and that the high ions (O VI and Ne VIII) reside in a collisionally ionized phase. Such necessity of a collisionally ionized phase where the high ions arise has also been demonstrated for other Ne VIII absorbers (Tripp et al. 2011; Narayanan et al. 2009, 2011; Savage et al. 2005).

4.2. *Collisional Ionization*

As the photoionization models fail to produce the O VI and Ne VIII column densities observed, we include a hot collisionally ionized phased as well. We assume that gas is in collisional ionization equilibrium (CIE), and that the hot phase has the same metallicity as the photoionzed material. As the profiles of O IV, OVI, and Ne VIII are all well aligned in velocity space , the assumption that the hot gas has the same metallicity as the photoionzed gas seems reasonable.

The steeply increasing Ne^{7+} and steeply declining O^{5+} ionization ratios in CIE as shown in the right side of Figure 11 allow for a precise temperature of the hot gas to be determined for the systems investigated here. With the temperature determined from the ratio of Ne VIII to O VI, the total hydrogen column density is determined by scaling the N_H^{tot} to match the observed column densities of Ne VIII and O VI. We find that log T$\sim$5.7 for these systems, similar to other absorption line systems with detected Ne VIII (Savage et al. 2005; Narayanan et al. 2009, 2011; Tripp et al. 2011).

We have also investigated the non-equilibrium collisional ionization models of Gnat & Sternberg (2007). Again, no single-phase model can account for the observed ratios of O III, O IV, O VI, and Ne VIII. Temperatures of log T$\sim$5.7 are also predicted in the non-equilibrium models based on the Ne VIII/O VI ratio.

The Doppler parameters of the lines also provide a constraint on the gas temperatures: $b = \sqrt{2kT/m}$ assuming the line profile is dominated by broadening from thermal motions in the cloud. This is effectively an upper limit of course, as turbulent motions can also contribute to the width of the profile. For log T$\sim$5.7 K as indicated by the Ne VIII/O VI ratios in these systems, the minimum Doppler parameter is $b_{O\ VI} > 22.7$ km s$^-1$ or $b_{Ne\ VIII} > 20.6$ to support the collisional ionization scenario. The Doppler parameters for all of the Ne VIII line in these systems are in agreement with the above constraint. The best fit Doppler parameters for the O VI $\lambda\lambda$ 1031, 1037 lines in the z_{abs}=0.6838 and z_{abs}=0.7105 systems are also fully consistent with collisional ionization. The z_{abs}=0.7248 system (which suffers from particularly noisy profiles) is slightly more discrepant, but still consistent within 2σ of the best fit Doppler parameter.

5. RESULTS

5.1. *Physical Conditions*

As the modified background spectra described above do not reproduce the observed column densities, we proceed under the assumption that the clouds are illuminated with the background radiation field of Haardt & Madau (2001).

The extragalactic background spectrum of Haardt & Madau (2001) has an ionizing photon flux ($h\nu > 13.6$ eV) of 2.2×10^5 photons s^{-1} cm^{-2} at $z \sim 0.7$. The background intensity does vary slightly between $z = 0.68$ and $z = 0.72$, however for the ease of the calculations we assume the above value for all the systems. We estimate the density and cloud sizes of the photoionized portion of the gas as the ionization parameter U relates the photon flux (given by the ionizing background spectrum of Haardt & Madau 2001) to the density of the gas. We find that $n \sim 10^{-4}$ cm^{-3} for these systems, corresponding to overdensities of $\Delta \sim 80$ at $z = 0.7$ ($\Delta = \rho/\bar{\rho}_b$). Variations in the intensity of the ionizing background would affect the densities determined here. The ionizing photon flux ϕ is of course unknown, and almost certainly varies from place to place in the Universe with enhancements from local sources. It has been argued however that the local contributions are negligible for systems with log N(H I)<17.0 (Schaye 2006). Results for the photoionized portion of the absorbers traced by species such as H I, O III, C III and O IV are given in Table 8.

We can predict the properties of the thermally broad-

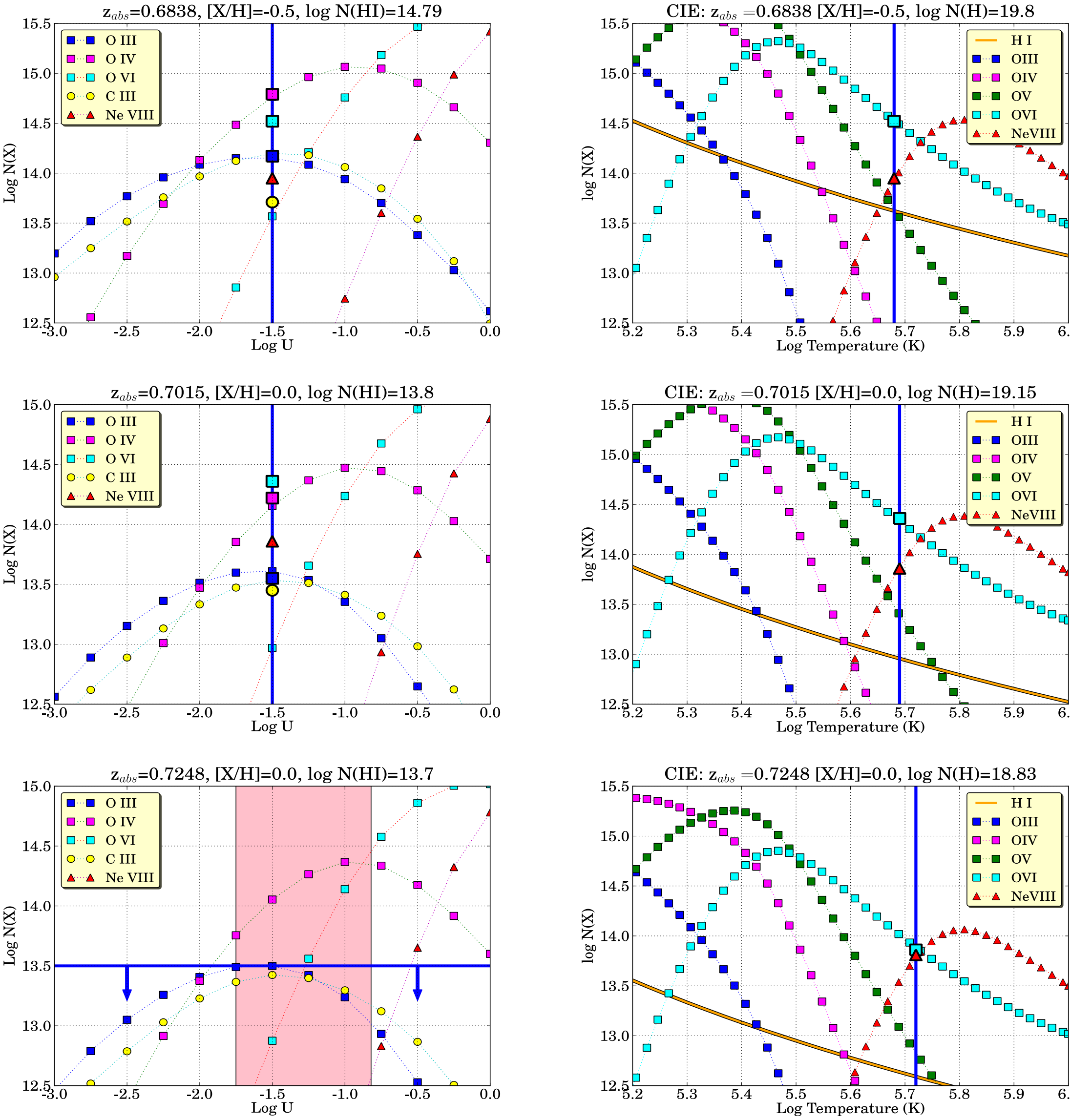

Figure 11. From top to bottom, photo (left side) and collisional (right side) ionization modeling for the systems is shown for the z_{abs}=0.6838, z_{abs}=0.7015, and z_{abs}=0.7248 systems. For the z_{abs}=0.6838 and z_{abs}=0.7015 systems, the measured column densities are shown in large points along the vertical blue line which denotes the best fitting ionization parameter or temperature. For the z_{abs}=0.7248 system, the shaded pink area marks the allowed values of log U based on the O III, O IV, and O VI column densities.

ened Lyman α lines in the collisionally ionized component in these systems implied by the CIE models described in §4. The Ne VIII/O VI ratio gives a unique temperature for the hot phase of the gas bearing O VI and Ne VIII. The Doppler parameters for H I are predicted to be 89-93 km s^{-1} at temperatures of log T$\sim$5.7. The thermally broadened Lyman α lines are likely to be difficult to detect for these systems for the following reasons. The optical depth at line center can be determined given the Doppler parameter and atomic data as

$$\tau_0 = 1.497 \times 10^{-15} \frac{N(cm^{-2}) f \lambda_0(\text{Å})}{b(km\ s^{-1})} \quad (1)$$

For the z_{abs}=0.6838 system, the thermally broadened Lyman α line may be potentially observable, with a optical depth at line center of $\tau_0 = 0.38$. This however is slightly misleading, as the Ne VIII and H I are well aligned in this system, so the broad feature will be superimposed on the much stronger Lyman α line from the photoionized gas. For the z_{abs}=0.7015 and z_{abs}=0.7248 systems, the optical depth at line center is only $\tau_0 < 0.07$; high S/N spectra may be able to able to detect such a feature but small undulations in the QSO continuum make broad and weak features hard to detect. Parameters for the collisionally ionized phase of the absorbers are given in Table 9.

5.2. *Redshift Density and Baryonic Content*

The COS spectrum of PG1148+549 enables detection of the redshifted Ne VIII $\lambda\lambda$ 770,780 lines above $z = 0.49$, and we exclude a 3000 km s^{-1} region at the emission redshift of the QSO to not include any possible absorbers associated with the QSO itself (Tripp et al. 2008). As the number of absorption lines in this spectrum is high, one must take into account the effects of line blanketing on the determination of the total absorption path length given in the equation above. Following the method outlined in Tripp et al. (2008) to account for such effects and variable S/N, we find $\Delta X = 0.81$ and $\Delta z = 0.41$ for a 10 pixel wide line and a minimum detection threshold of 20 mÅ, corresponding to the smallest observed equivalent width for the weaker line of the Ne VIII doublet in these systems.

We estimate the redshift density of Ne VIII absorbers to be $\mathrm{d}\mathcal{N}/\mathrm{d}z \sim 7^{+7}_{-3}$ for $W_0 > 30m$Å given the three absorbers detected in this spectrum over a total redshift path of $\Delta z = 0.41$. We assume Poisson statistics in the determination of our confidence intervals, with values taken from (Gehrels 1986). This estimate will be revised in future work when all of the spectra from this program will be analzed and presented. We note that the redshift density of O VI absorbers is only slightly greater than the estimate above for Ne VIII absorbers, with $\mathrm{d}\mathcal{N}^{OVI}/\mathrm{d}z \sim 5-9$ for O VI systems with equivalent widths similar to the systems here of EW(1031)$\gtrsim$ 80 mÅ (Tripp et al. 2008).

We can make an estimate of the total comoving density traced by the O VI and Ne VIII absorbers from these observations. The comoving gas density is related to the column densities in the absorbers as

$$\Omega_g = \frac{H_0}{c}\frac{\mu m_H}{\rho_c}\frac{\sum_i^n N_i}{\Delta X} \qquad (2)$$

where ΔX is the absorption path length in a flat cosmology defined as

$$\Delta X = \int_{z1}^{z2} \frac{(1+z)^2}{\sqrt{\Omega_m(1+z)^3+\Omega_\Lambda}} dz \qquad (3)$$

(Wolfe, Gawiser & Prochaska 2005).

Using the N(H_{tot}) values determined in Section 4 from matching the observed O VI and Ne VIII column densities in CIE, we find that the density of gas as traced by these absorbers is $\Omega_{gas} = 0.002$, or roughly 4% of the baryon density determined by observations of the cosmic microwave background (Spergel et al. 2007). This is a crude estimate, and will be updated when the full sample of Ne VIII absorbers in the program are analyzed. As $\sim$ 50% of the baryons at low z are unaccounted for (Fukugita et al. 1998), there is still a sizable fraction of baryons missing.

5.3. *Sizes and Stability*

From the definition of the redshift density,

$$\frac{d\mathcal{N}}{dz} = n\pi R^2 \frac{c}{H(z)}(1+z)^2, \qquad (4)$$

the number density of absorbers n is directly related to the redshift density $\mathrm{d}\mathcal{N}/\mathrm{d}z$ and cross sectional area of the absorbing cloud. Under the assumption that these systems are connected to the CGM in the halos of galaxies, which seems likely as O VI systems have been clearly linked to the CGM of galaxies at lower redshifts (Tumlinson et al. (2011b); Prochaska et al. (2011), but see also Tripp et al. (2006)), we can estimate the typical sizes of the collisionally ionized clouds bearing O VI and Ne VIII from the observed redhsift density $\mathrm{d}\mathcal{N}/\mathrm{d}z$ and number density of galaxies ϕ at $z \sim 0.7$.

The galaxy luminosity function is well constrained at the redshift of the systems in this work (Ilbert et al. 2005). The survey of Ilbert et al. (2005) is reasonably complete down to $0.1\mathrm{L}_\star$ at $z = 0.7$, as such, we take this as the lower bound in the integration over the luminosity function. The inclusion of lower luminosity galaxies would of course increase the overall number density, however deep spectroscopic galaxy surveys of fields with known O VI absorbers indicate that dwarf galaxies ($\mathrm{L} < 0.\mathrm{L}_\star$) are unlikely to have a high covering fraction of O VI in their halos (e.g. Prochaska et al. 2011; Wakker & Savage 2009), and are hence unlikely to have an impact on the calculation.

Taking the R-band Schechter function parameters of $\mathrm{M}_\star = -22.62$, $\phi_{star} = 1.9\times10^{-3}$, and $\alpha = -1.41$ from (Ilbert et al. 2005), we find that $n(L > 0.1L_\star) = 2.4\times 10^{-2}$. This is turn yields characteristic sizes for the O VI+Ne VIII systems of $\sim 70-150$ kpc. Such sizes are quite similar to what has been determined for the sizes of the halos of lower redshift galaxies via absorption line statistics (Tumlinson et al. 2011b; Prochaska et al. 2011; Wakker & Savage 2009).

For the photoionized portions of the clouds, we can estimate the stability to collapse as we have both a density and size from the photoionization modeling. The Jeans length gives the characteristic length scale for which a cloud can be stable against gravitational fragmentation and collapse. Given a gas fraction f_g, density n_{HI}, and temperate T, the Jeans length is given by (Schaye 2001)

$$L_J \sim 6.5\times10^4\ pc\Big(\frac{n_{HI}}{10^{-4}\ cm^{-3}}\Big)^{-1/2}\Big(\frac{T}{10^4\ K}\Big)^{1/2}\sqrt{f_g} \qquad (5)$$

The CLOUDY simulations described in §4 determined temperatures of $T \sim 2\times10^4$ K for the photoionized gas, combined with the densities given above of $n_H \sim 2\times10^{-4}$ gives Jean's lengths of $L_J \sim 65$ kpc assuming that the clouds are gas dominated. All of the systems in this work are constrained to have sizes well below L_J, implying that the ultimate fate of these systems is to evaporate into the surrounding medium (unless they are confined by some other mechanism). Similar such metal rich, compact clouds have also been observed at high redshift (Schaye et al. 2007).

6. AFFILIATED GALAXIES

We have obtained deep multiband imaging of the PG1148+549 field with the Large Binocular Telescope (LBT) and Large Binocular Camera (LBC). The U-band image of the field centered on the QSO is shown in Figure 12. The data have a limiting magnitude of $m_U < 27$. Spectra of galaxies labelled 76_24 and 142_30 were obtained with the Keck Low Resolution Imaging Spectrometer (LRIS). The data were reduced and analysed as described in (Werk et al. 2011). Parameters for the galaxies labelled in Figure 12 are given in Table 10.

Strong absorption from C III λ 977, O VI $\lambda\lambda$ 1031, 1037, and multiple Lyman series lines are seen at z_{abs}=0.2525 associated with galaxy 76_24. More interesting for this work, the galaxy 142_30 is only $\Delta v \sim +30$ km s^{-1} from the absorber at z_{abs}=0.7248. This galaxy is bright, with L$\sim$L*, has a high metallicity

Table 8
Conditions in the photoionized gas of the $z \sim 0.7$ absorbers.

Redshift	log N(H I) cm^{-2}	log N(H$_{tot}$) cm^{-2}	log U	[X/H]	Density cm^{-3}	Size kpc
0.6838	14.79±0.03	18.80	-1.5	-0.5	2×10^{-4}	10
0.7015	< 13.8	<17.69	-1.5	> 0.0	2×10^{-4}	< 1
0.7248	< 13.7	< 18.46	-1.75 to -0.75	> -0.5	$(0.4\text{-}4.0)\times10^{-4}$	< 23

Table 9
Parameters for the collisionally ionized gas of the $z \sim 0.7$ absorbers.

Redshift	log T K	log N(H$_{tot}$) cm^{-2}	log N(H I)^{a} cm^{-2}	b$^{b}_{pred}$ km s^{-1}	τ^{c}_{0}
0.6838	5.68	19.80	13.65	89	0.38
0.7015	5.69	19.15	12.90	90	0.07
0.7248	5.72	18.83	13.08	93	0.10

[a] The predicted neutral hydrogen column density given the temperature and N(H$_{tot}$).
[b] The predicted Doppler parameter for hydrogen at the given temperature.
[c] The predicted optical depth at line center for Lyman α for the column density and Doppler parameter.

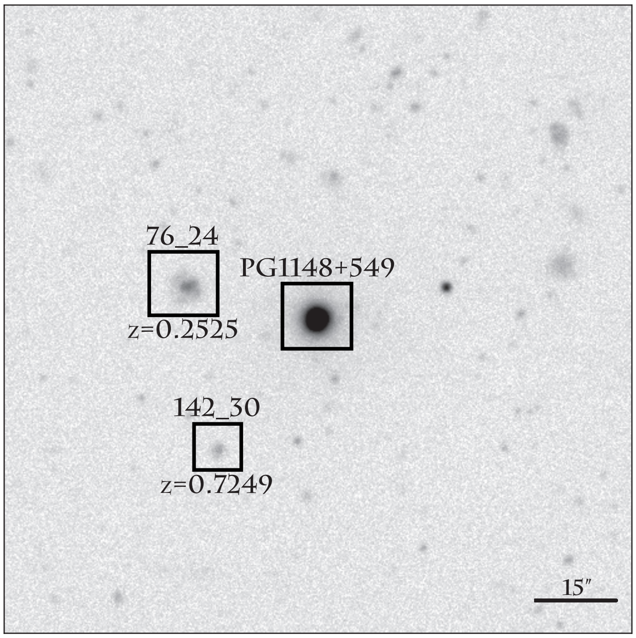

Figure 12. A deep U band image of the PG1148+549 field centered on the QSO. Galaxies for which we have obtained spectroscopic redshifts are labeled according to their position angle and distance in arcseconds from the QSO.

of [O/H]=+0.22±0.15, and a relatively high SFR of 6.42±0.44 M$_{\odot}$ yr^{-1}. The LRIS spectrum of this galaxy is shown in Figure 13.

This high metallicity is consistent with the constraints on the metallicity of the absorption system of [O/H]> 0.0. Similarly, the high star formation rate is consistent with the recent findings of Tumlinson et al. (2011b) and Prochaska et al. (2011) that O VI is ubiquitously observed in the halos of star forming galaxies. Several other galaxies are also clearly seen in Figure 12. A more complete redshift survey of these galaxies is required to eliminate the possibility of other galaxies at the absorption redshift as well.

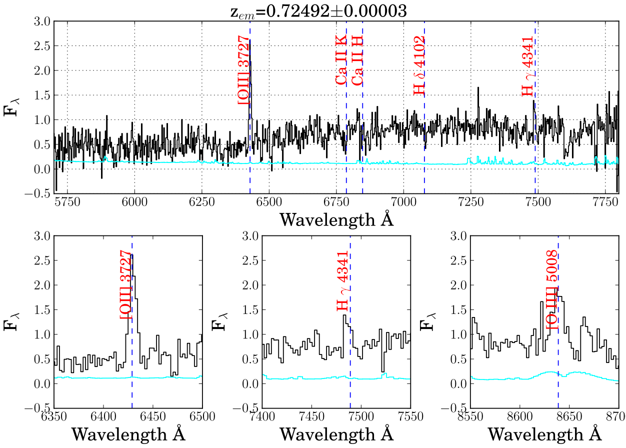

Figure 13. Keck/LRIS spectrum of the galaxy located at $z_{em} = 0.7248$ at an impact parameter of 217 kpc. Prominent spectral features are labeled. The cyan line below the spectrum represents the 1σ error in the flux.

7. SUMMARY AND DISCUSSION

In this work we have reported on the physical conditions and ionization in the Ne VIII + O VI absorbers in the COS spectrum of PG1148+549. We summarize the results as follows:

1. A single-phase model in which all of the ions are produced via photoionization or collisional ionization fails to reproduce the observed column density ratios. Models in which the high ions are produced via photoionization predict unphysically large cloud sizes, with absorption lines that would be dominated by Hubble broadening. We conclude that the O VI and Ne VIII arise in collisionally ionized gas with T∼ $10^{5.7}$ K, while the low ions are produced via photoionization.
2. The metallicities of the systems, as determined from the low ions and photoionization modeling, are all [O/H]> -0.5, higher than the typically assumed metallicity of the IGM of [X/H]∼ -1.0. The z_{abs}=0.7015 and z_{abs}=0.7248 systems indicate supersolar metallicities.
3. We have investigated the consequences of modifying the ionizing background of (Haardt & Madau 2001). We have attempted to include an obscured AGN with a soft X-Ray cutoff at 100 eV, which would boost the flux near the ionization potentials required to produce O VI and Ne VIII. Even with these significant modifications to the extragalactic background of Haardt & Madau (2001), the models fail to produce the observed O VI and Ne VIII column densities.
4. We have determined that the gas as traced by O VI and Ne VIII has temperatures of T∼ $10^{5.7}$ K

via the O VI to Ne VIII ratio in collisional ionization equilibrium. Non-equilibrium models of Gnat & Sternberg (2007) also give similar temperatures based on the O VI to Ne VIII ratio.

5. Densities of $n_H \sim 10^{-4}$ cm^{-3}, corresponding to overdensities of $\Delta \sim 80$ at $z = 0.7$ are determined from the photoionization modeling. The photoionzed portions of the clouds are compact, with sizes R$\lesssim$ 10 kpc.
6. The Jean's length for the photoionized portion of these systems are $L_J \sim 65$ kpc, much larger than the derived cloud sizes. The clouds are thus not gravitationally bound, and will evaporate while enriching the IGM and CGM with metals.
7. We determine the redshift density of Ne VIII absorbers to be d$\mathcal{N}$/d$z$$\sim 7^{+7}_{-3}$ for W$_0 > 30m$Å, with a cosmic baryon density of $\Omega_{gas} = 0.002$, or roughly 4% of the baryon density determined by observations of the cosmic microwave background. A large fraction of the baryons are thus still unaccounted for.
8. Based on the observed redshift density and galaxy luminosity function at $z \sim 0.7$, we estimate the characteristic size of the collisionally ionized gas harboring the O VI + Ne VIII absorbers to be $\sim 70 - 150$ kpc.
9. We find a luminous star forming galaxy at an impact parameter of $\sim$ 220 kpc from the z_{abs}=0.7248 system. The galaxy also has a high metallicity, linking the absorpion line system to the hot extended halo of the galaxy.

It is interesting that the profiles of the O III, O IV, and O VI are well aligned (in the sense that the component structure is similar for all the lines), but a single-phase model consisting of only photoionization or collisional ionization fails to reproduce the observed column densities. Based on the ionization modeling we are forced to conclude that the highly ionized species of O VI and Ne VIII are not created in by pure photoionization in these systems.

Turbulent mixing layers are another mechanism in which to create highly ionized ions in the halos of galaxies. In this scenario, cool, dense material is mixed with hot ($\sim 10^6$ K) gas as the materials slide past each other (Begelman & Fabian 1990; Slavin & Cox 1993; Kwak & Shelton 2010). Kelvin-Helmholtz instabilities in the gas create a mixing of the phases and the mixed gas produces elevated amounts of high ions than collisional ionization equilibrium (Kwak & Shelton 2010; Kwak et al. 2011).

Recent COS observations indicate a near unity filling factor for O VI within 150 kpc of star forming galaxies (Tumlinson et al. 2011b). If we assume a typical cloud size of 10 kpc similar to what we have determined here, $\sim$200 individual clouds would be necessary along a given line of sight to ensure that the covering fraction is near unity. The small cloud sizes determined here for the photoionzed gas as traced by species such as H I, O III, and O IV would require many clouds in order to produce a high filling factor such as is seen in (Tumlinson et al. 2011b). If the O VI arises in a thin skin on the surface of the lower-ionization clouds, then the size of the O VI cloud would be effectively similar to that of the low-ionization phase. Such a scenario would also likely lead to much more complex profiles than what is typically seen (some systems do however show remarkably complex profiles in O VI however Tumlinson et al. (2011a)).

Table 10
Parameters for the galaxies with spectroscopic redshifts shown in 12

ID	z_{em}	ρ	SFR	M$_r$	[O/H]
		kpc	M$_\odot$ yr^{-1}		
76_24	0.25250	95	1.53±0.04	-19.86 ± 0.04	-0.11 ± 0.15
142_30	0.72492	217	6.42±0.44	-21.15 ± 0.13	$+0.22 \pm 0.15$

The turbulent mixing layer scenario, while it does produce elevated levels of high ions, would still require many clouds in order to account for the large filling factor of O VI seen in Tumlinson et al. (2011b) as the high ions are produced on the skins of the clouds. One possible explanation is that the O VI is resulting from the evaporation of the outer parts of the clouds expanding into the halo of the galaxy, leaving behind a smaller and less ionized cloud that is traced by H I, Mg II, C II, etc. It is also unclear if the turbulent mixing layers would be effective at large impact parameters to the galaxies, where the densities are low and mixing would therefore less effective.

Much effort has been made recently into simulations of structure formation including the enrichment of the IGM via galaxy feedback with hydrodynamical simulations (Tepper-Garcìa et al. 2011; Davé et al. 2001; Oppenheimer & Davé 2006, 2009; Oppenheimer et al. 2011). The origins of the O VI absorbers is of much debate. Some simulation indicate that the O VI absorbers are mainly collisionally ionized (e.g. Cen & Chisari 2011), while others point to photoionization as the main mechanism producing O VI (e.g. Oppenheimer & Davé 2009; Oppenheimer et al. 2011). Some simulations also indicate that the stronger systems with EW> 100 mÅ are more likely to be collisionally ionized (Cen et al. 2001; Fang & Bryan 2001; Oppenheimer & Davé 2009; Oppenheimer et al. 2011). The observations presented here support a collisional ionization mechanism for the O VI and Ne VIII, in general agreement with the hydrodynamic simulations as the equivalent widths of the O VI lines are among the stronger systems that arise in the simulations.

The metallicities of O VI absorbers are similarly disparate in the simulations. The simulations of Tepper-Garcìa et al. (2011) and Oppenheimer & Davé (2009) indicate that most of the O VI absorbers reside in metal enriched regions with $-1.0 <[Z/Z_\odot]<0.0$, whereas in Cen & Chisari (2011) the metallicities of the O VI absorbers is much lower, with $-2.5 <[Z/Z_\odot]< -0.5$. The metallicities determined here, as well as other systems in for which there are multiple ionization states to adequately constrain the ionization models similarly indicate metallicities of [O/H]$\gtrsim -0.5$ (Howk et al. 2009; Narayanan et al. 2011; Savage et al. 2005; Tripp et al. 2011).

Based on a large sample of QSOs, Tripp et al. (2008) find a redshift density of d$\mathcal{N}^{OVI}$/d$z$$\sim 5 - 9$ for systems with W$_0 > 100$ mÅ. The similar value determined for the Ne VIII systems of d$\mathcal{N}^{NeVIII}$/d$z$$\sim 7$ perhaps indicates that many O VI systems could harbor Ne VIII lines.

Ne VIII may only be detectable in the strongest O VI absorbers as the neon abundance is lower than that of oxygen by a factor of ∼7 (Lodders 2003).

As was noted in the previous sections, the exact shape of the ionizing background is unknown and a limiting factor when determining the metallicities and physical conditions in QSO absorption systems. With multiple ions of the same element, or perhaps multiple ions of several elements which have little intrinsic scatter in their relative abundances, it may be possible to measure the shape of the ionizing background radiation directly based on the relative proportions of column densities in different ionization stages. Oxygen and sulfur could be possibly be utilized simultaneously as both are α-elements with multiple ionization stages present in the FUV. We plan to investigate this possibility further in future work.

ACKNOWLEDGMENTS

J.D.M. would like to thank R. J. Farnsworth and P. Chop for their enlightening discussions. Special thanks to Cristina Williams for technical assistance. Financial support for this research was provided by NASA grants HST-GO-11598.03-A and NNX08AJ44G. J.X.P. also acknowledges support from NSF grant (AST-0709235).

REFERENCES

Akerman C.J., Carigi L., Nissen P.E., Pettini M., Asplund M., 2004, A&A, 414, 931
Anderson M.E., Bregman J.N., 2010, ApJ, 714, 320
Begelman M. C., Fabian A. C. 1990, MNRAS, 244, 26P
Blanton M.R., Hogg D.W., Bahcall N.A., Brinkman J., Britton M., Connolly A.J., Csabai I., Loveday J., et al., 2003, ApJ, 592, 819
Bowen D.V., et al., 2008, ApJS, 176, 59
Bregman J.N., 2007, ARAA, 45, 221
Bregman J.N., Otte B., Irwin J.A., Putman M.E., Lloyd-Davies E.J., Brüns C.,2009, ApJ, 699, 1765
Cen R., Tripp T. M., Ostriker J. P., Jenkins E. B. 2001, ApJ, 559, L5
Cen R., Fang T., 2006, ApJ, 650, 573
Cen R., Chisari N. E., 2011, ApJ, 731, 11
Chen H.-W., Prochaska J.X., 2000, ApJ, 543, 9
Danforth C. W., Stocke J.T., Shull J.M., 2010, ApJ, 710, 613
Davé R., et al. 2001, ApJ, 552, 473
Fang T., Bryan G. L. 2001, ApJ, 561, L31
Ferland G. J., Korista K.T., Verner D.A., Ferguson J.W., Kingdon J.B., Verner E.M., 1998, PASP, 110, 761
Froning C.S., Green J.C., Ap&SS, 320, 181
Fukugita M., Hogan C.J., Peebles P.J.E., 1998, ApJ, 503, 518
Fukugita M., Peebles P.J.E., 2004, ApJ, 616, 643
Gehrels N., 1986, ApJ, 303, 336
Ghavamian, P., et al. 2009, Preliminary Characterization of the Post-Launch Line Spread Function of COS, `http://www.stsci.edu/hst/cos/documents/isrs/`
Gant O., Sternberg A., 2007, ApJS, 168, 213
Green J., et al., 2011, (arXiv:1110.0462)
Haardt F., Madau P., 1996, ApJ, 461, 20
Haardt F., Madau P., in 21st Moriond Astrophysics Meeting, Clusters of Galaxies and the High Redshift Universe Observed in X-rays, Recent Results of XMM-Newton and Chandra, ed. D. M. Neumann, J. T. T. Van
Heckman T.M., Dahlem M., Lehnert M.D., Fabbiano G., Gilmore D., Waller W.H., 1995, ApJ, 448, 98
Howk J.C., Ribaudo J.S., Lehner N., Prochaska J., Chen H-W., 2009, MNRAS, 396, 1875
Ilbert O., et al., 2005, A&A, 2005, 439, 863
Kwak K., Shelton R.L., 2010, ApJ, 719, 523
Kwak K., Henley D.B., Shelton R.L, 2011, ApJ, 739, 30
Lehner N., Savage B. D., Richter P., Sembach K. R., Tripp T. M., Wakker B. P., 2007, ApJ, 658, 680
Lehner N., et al., 2009, ApJ, 694, 734
Li J.-T., Li Z., Wang Q.D., Irwin J. A., Rossa J., 2008, MNRAS, 390, 59
Lodders, K., 2003, ApJ, 591, 1220
Maller A.H., Bullock J.S., 2004, MNRAS, 35, 694
Martin C.L., Kobulnicky H.A., T.M., 2002, ApJ, 574, 663
McGaugh S.S., Schombert J.M., De Blok W.J.G., Zagursky M.J., 2010, ApJ, 708, L14
Meiring J.D., Tripp T.M., Prochaska J.X., Tumlinson J., Werk J., Jenkins E.B., Thom C., O'Meara J.M., Sembach K.R., 2011, ApJ, 732, 35
Morton D.C., 2003, ApJS, 149, 205
Narayanan A., et al., 2011, ApJ, 730, 15
Narayanan A., Wakker B. P., Savage B. D. 2009, ApJ, 703, 74
O'Meara J. M., Burles S., Prochaska J. X., Prochter G. E., Bernstein R. A., Burgess K. M., 2006, ApJ, 649, L61
Oppenheimer B.D., Davé R., 2006, MNRAS, 373, 1265
Oppenheimer B.D., Davé R., 2009, MNRAS, 395, 1875
Oppenheimer B.D., Davé R., Katz N., Kollmeier J.A., Weinberg D.H., 2011, MNRAS, in press
Peng C.Y., Ho L.C., Impey C.D., Rix H-W., 2010, AJ, 139, 2097
Pettini M., Zych B.J., Steidel C.C., Chaffee F.H., 2008, MNRAS, 385, 2011
Prochaska J.X., Weiner B., Chen H.-W., Mulchaey J., Cooksey K., 2011, ApJ, 740, 91
Raymond J.C., 1992, ApJ, 384, 502
Savage B.D., Sembach K.R., 1991, ApJ, 151, 313
Savage B. D., Lehner N., Wakker B. P., Sembach K. R., Tripp T. M. 2005, ApJ, 626, 776
Savage B.D., Narayanan A., Lenher N., Wakker B.P., 2011, ApJ, 731, 14
Schaye J., 2001, ApJ, 559, 507
Schaye J., 2006, ApJ, 643, 59
Schaye J., Carswell R.F., Kim T.-S., 2007, MNRAS, 379, 1169
Schmidt M., 1963, ApJ 137, 758
Semback K.R., Tripp T.M., Savage B.D., Richter P., 2004, ApJS, 155, 351
Slavin J. D., Cox D. P., 1993, ApJ, 417, 187
Smith et al., 2011, ApJ, 731, 6
Spergel D.N., Bean R., Dore O., Nolta M.R., Bennett C.L., Dunkley J., Hinshaw G., Jarosik N., Komatsu E., Page L., 2007, ApJS, 170, 377
Thom C., Werk J.E., Tumlinson J., Prochaska J.X., Meiring J.D., Tripp T.M., Sembach K.R., 2011, ApJ, 736, 1
Tepper-Garcìa T., Richter P., Schaye J., Booth C.M., Vecchia C.D., Theuns T., Wiersma R.P.C., 2011, MNRAS, 413, 190
Tripp, T. M., Aracil, B., Bowen, D. V., & Jenkins, E. B. 2006, ApJ, 643, L77
Tripp T.M., Sembach K.R., Bowen D.V., Savage B.D., Jenkins E.B., Lehner N., Richter P., 2008, ApJS, 177, 39
Tripp T.M., et al., 2011, Science, 2011, 334, 952
Tumlinson J.T., Fang T., 2005, 623, L97
Tumlinson J.T., Werk J.K., Thom C.T., Meiring J.D., Prochaska J.X., Tripp T.M., Okrochkov M., Sembach K.R., 2011, 733, 111
Tumlinson J.T., et al., 2011, Science, 334, 948
Van Zee L., Salzer J.J., Haynes M.P., O'Donoghue A.A., 1998, ApJ, 116, 2805
Van Zee L., Haynes M.P., 2006, ApJ, 636, 214
Veilleux S., Cecil G., Bland-Hawthorn J., 2005, ARAA, 43, 769
Verner D.A., Barthel P.D., Tytler D., 1994, A&ASS, 108, 287
Wakker B.P., Savage B.D., 2009, ApJS, 182, 378
Werk J. K., et al., 2011, ApJ, in press
Wolfe A.M., Gawiser E., Prochaska J.X., 2005, ARAA, 43, 1, 861
Worthey G., Dorman B., Jones L.A., 1996, AJ, 112, 948